Supporting Information

Improving the Photovoltaic Performance of Fluorinated 2,2'-Bithiophene Core-based D(A-Ar)$_2$ Type Small Molecules via Strategically End-capped Heteroaromatic Substitution

Min Li,[b] Shichao Wang,[c] Chengjia Bao,[a] Zuoji Liu,[b] Dan Bai,[d]* Zhen Yang,[b]

Weiguo Zhu,[a]* Qiang Peng,[c]* Yu Liu,[a,b]*

[a]*School of Materials Science and Engineering, Jiangsu Collaboration Innovation Center of Photovoltaic Science and Engineering, Jiangsu Engineering Laboratory of Light-Electricity-Heat Energy-Converting Materials and Applications, National Experimental Demonstration Center for Materials Science and Engineering, Changzhou University, Changzhou 213164, P. R. China.*

[b]*College of Chemistry, Key Lab of Environment-Friendly Chemistry and Application in the Ministry of Education, Xiangtan University, Xiangtan 411105, China.*

[c]*Key Laboratory of Green Chemistry and Technology of Ministry of Education, College of Chemistry, and State Key Laboratory of Polymer Materials Engineering, Sichuan University, Chengdu 610065, China*

[d]*Department of Biochemistry and Molecular Biology, School of Medicine, Xi'an Jiaotong University, Xi'an, Shaanxi Province 710061, China*

Email addresses:

(Y. L) liuyu03b@126.com

(Q. P) qiangpeng@scu.edu.cn

(D.B) iamdbai@nwpu.edu.cn

(W. Z) zhuwg18@126.com

Contents

1. Characterization and measurement

Nuclear magnetic resonance (NMR) spectra were recorded on a Bruker AV-400 spectrometer using tetramethyl silane (TMS) as a reference in deuterated chloroform solution at 298 K. Mass spectrometric measurements were performed on Bruker Bifiex III MALDI-TOF. Thermogravimetric analyses (TGA) were conducted under a dry nitrogen gas flow at a heating rate of 20 ˚C min^{-1} on a Perkin-Elmer TGA 7. Differential scan calorimetry (DSC) measurements were carried out with a Netzsch DSC-204 under N_2 flow at heating and cooling rates of 10 °C min^{-1}. UV-Vis absorption spectra were recorded on a HP-8453 UV visible system. Cyclic voltammograms (CV) were carried out on a CHI660A electrochemical work station with three electrode electrochemical cell in a 0.1 M tetrabutylammonium hexafluorophosphate ($TBAPF_6$) acetonitrile solution with a scan 100 mV s^{-1} at room temperature (RT) under argon atmosphere. In this three-electrode cell, a platinum rod, platinum wire and Ag/AgCl electrode were used as a working electrode, counter electrode and reference electrode, respectively. The surface morphology of the SMs:$PC_{71}BM$ blend film was investigated by an atomic force microscopy (AFM) on a Veeco, DI multimode NS-3D apparatus in a tapping mode under normal air condition at RT with a 5 μm scanner. The HOMO and LUMO distributions of SMs were calculated by the density functional theory (DFT) (B3LYP; 6-31G*) method.

2. [1] H NMR and [13] C NMR Spectra

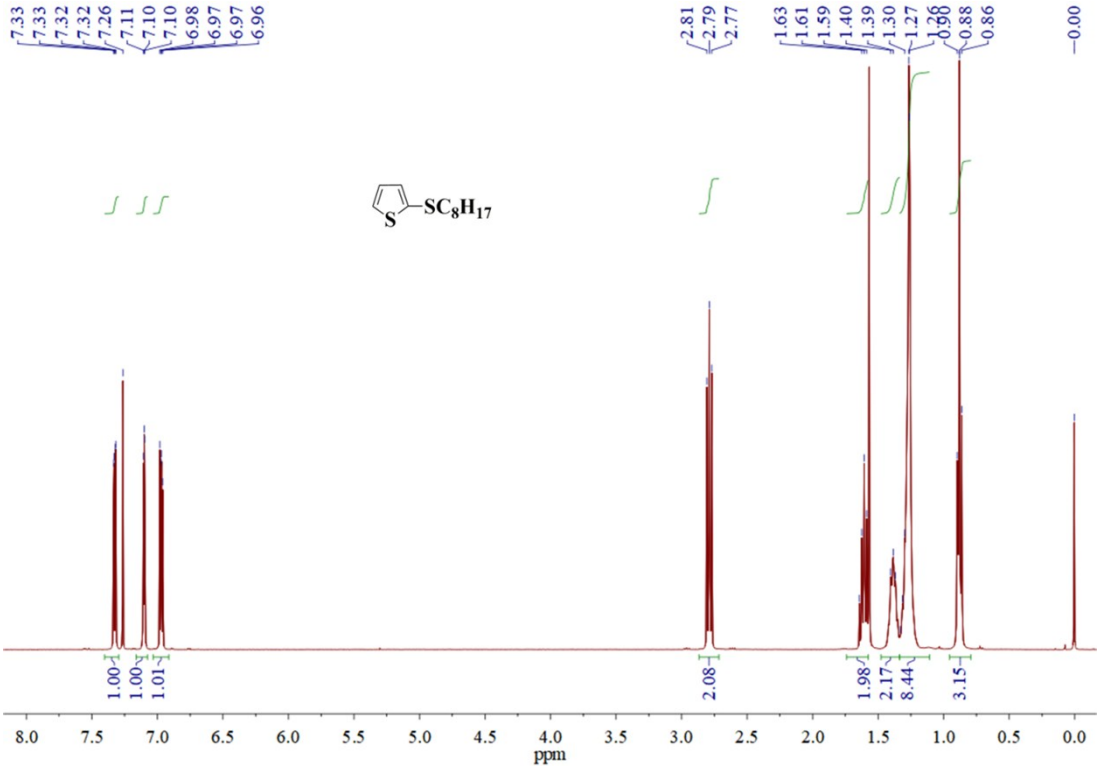

Fig.S1. [1]H NMR spectrum of TS.

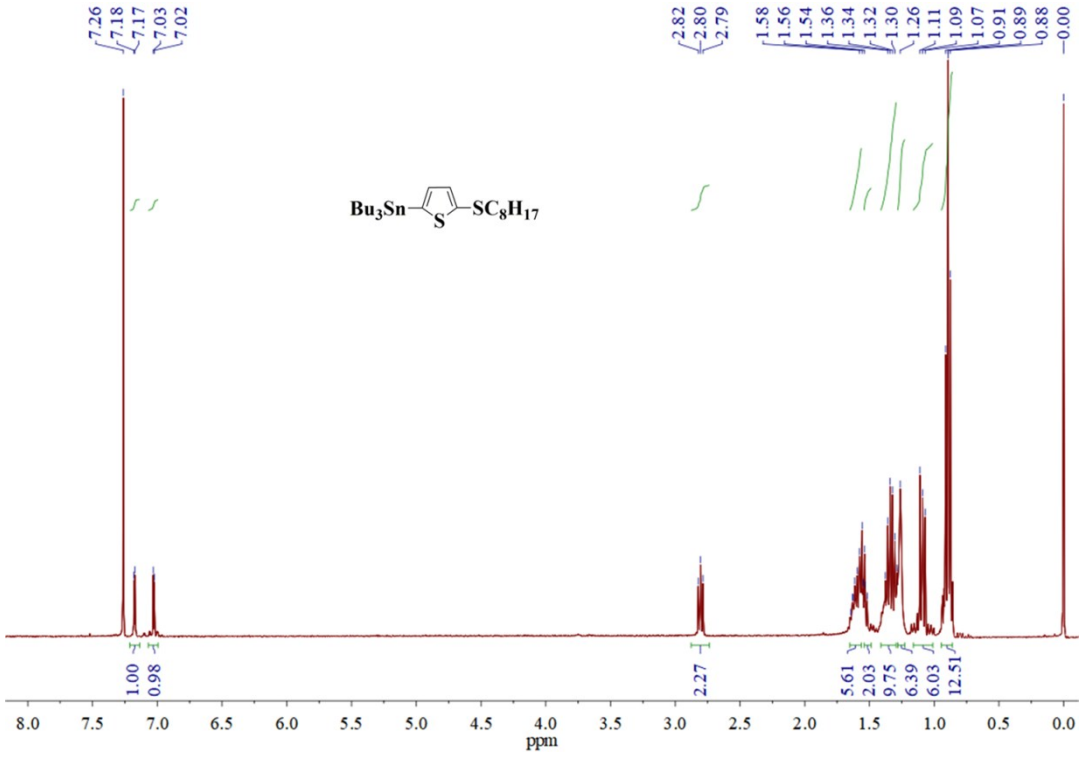

Fig. S2. [1]H NMR spectrum of product TS-Sn.

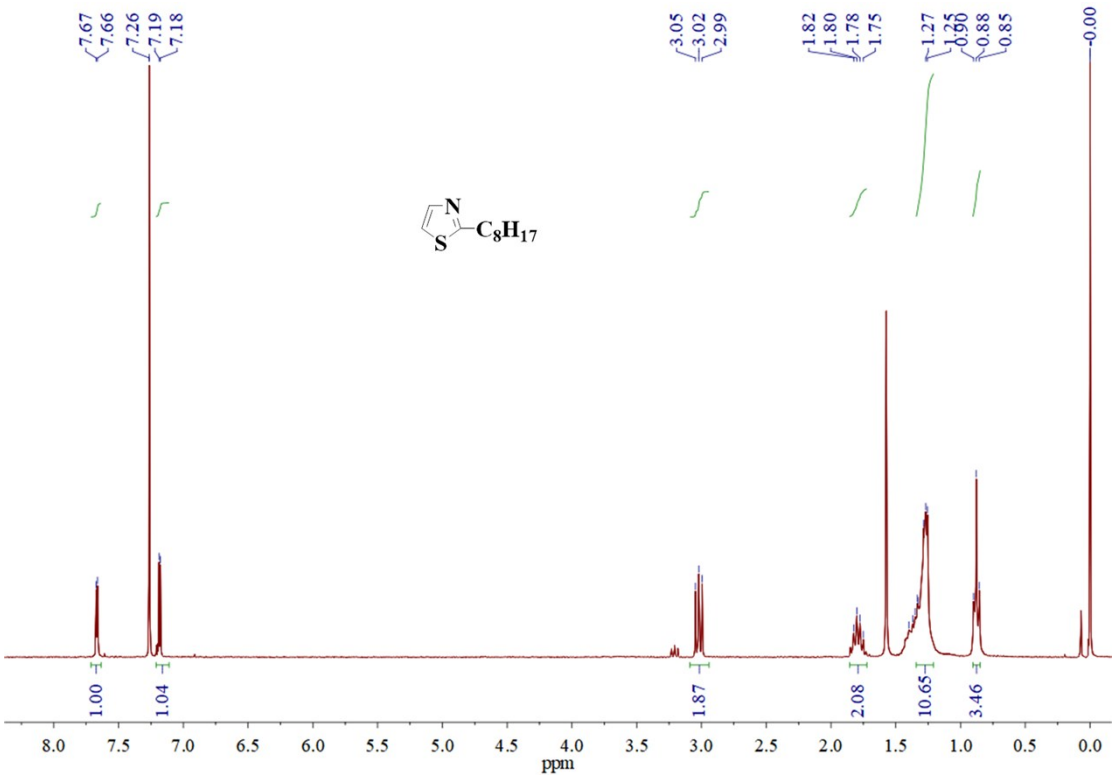

Fig.S3. [1]H NMR spectrum of TZ.

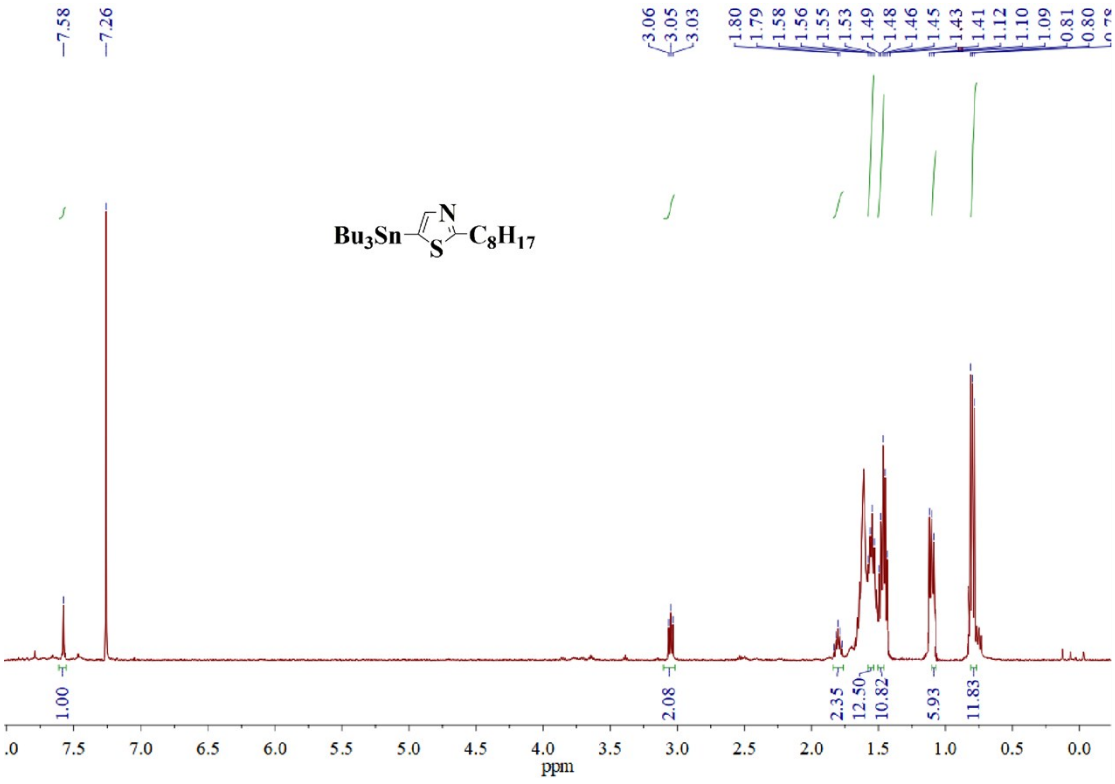

Fig.S4. [1]H NMR spectrum of TZ-Sn.

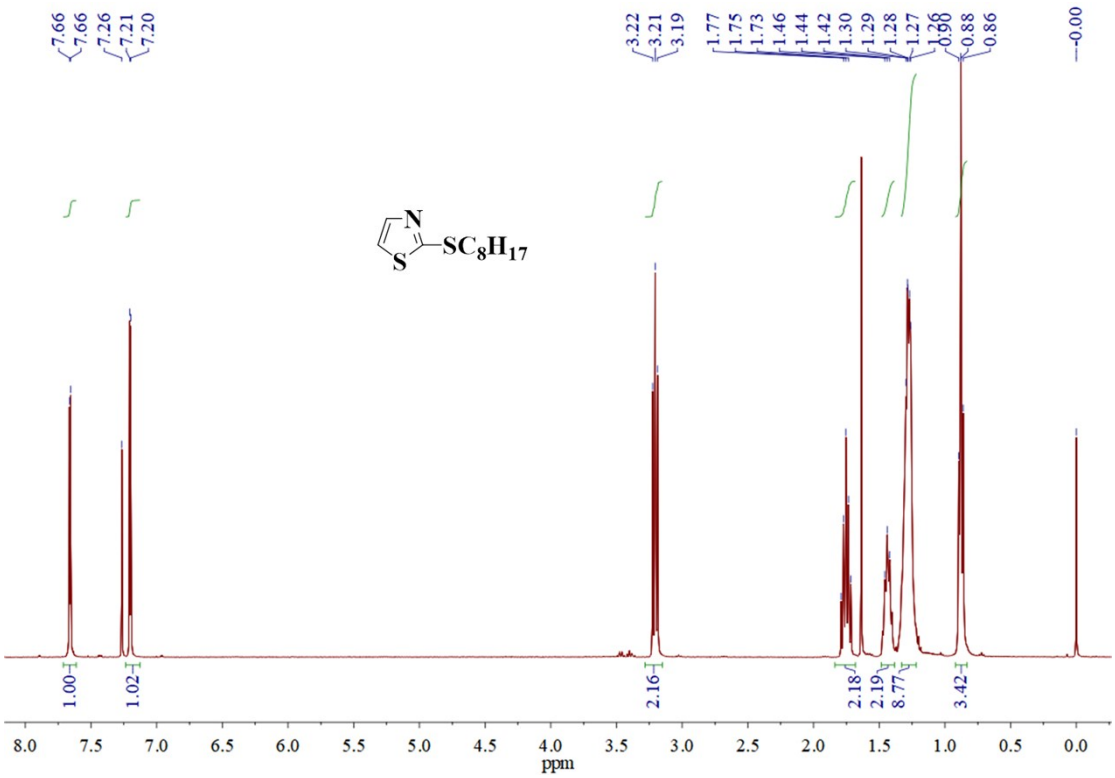

Fig.S5. [1]H NMR spectrum of TZS.

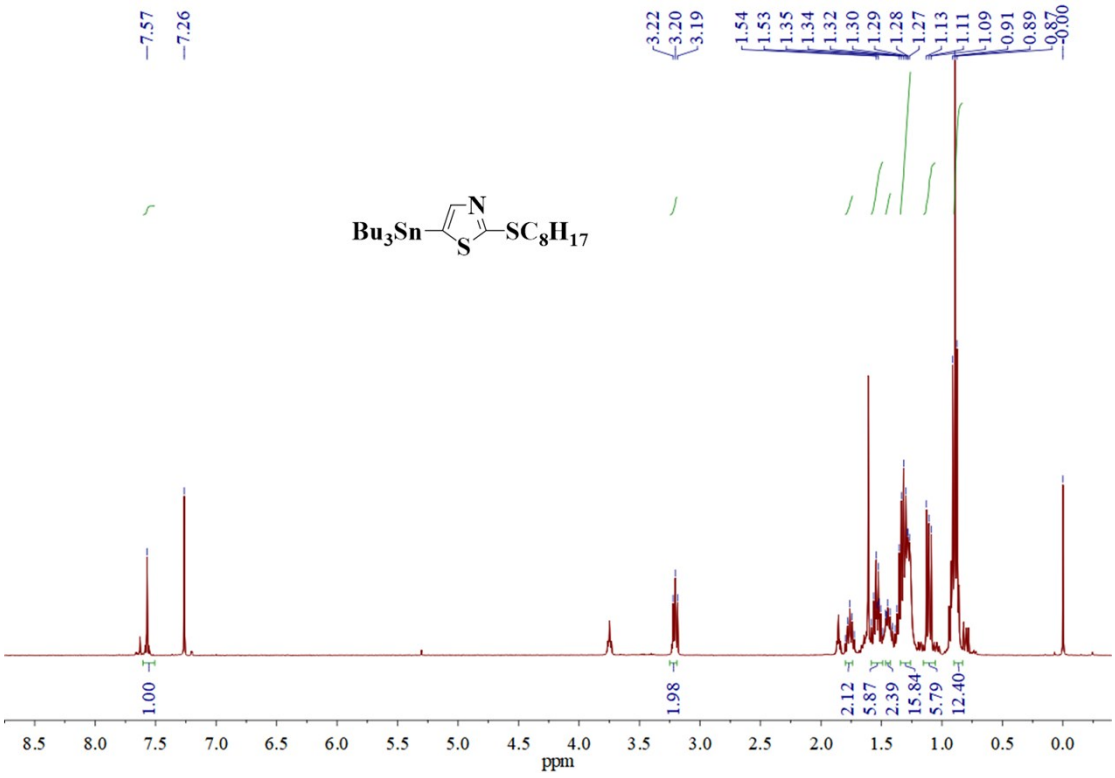

Fig.S6. [1]H NMR spectrum of TZS-Sn.

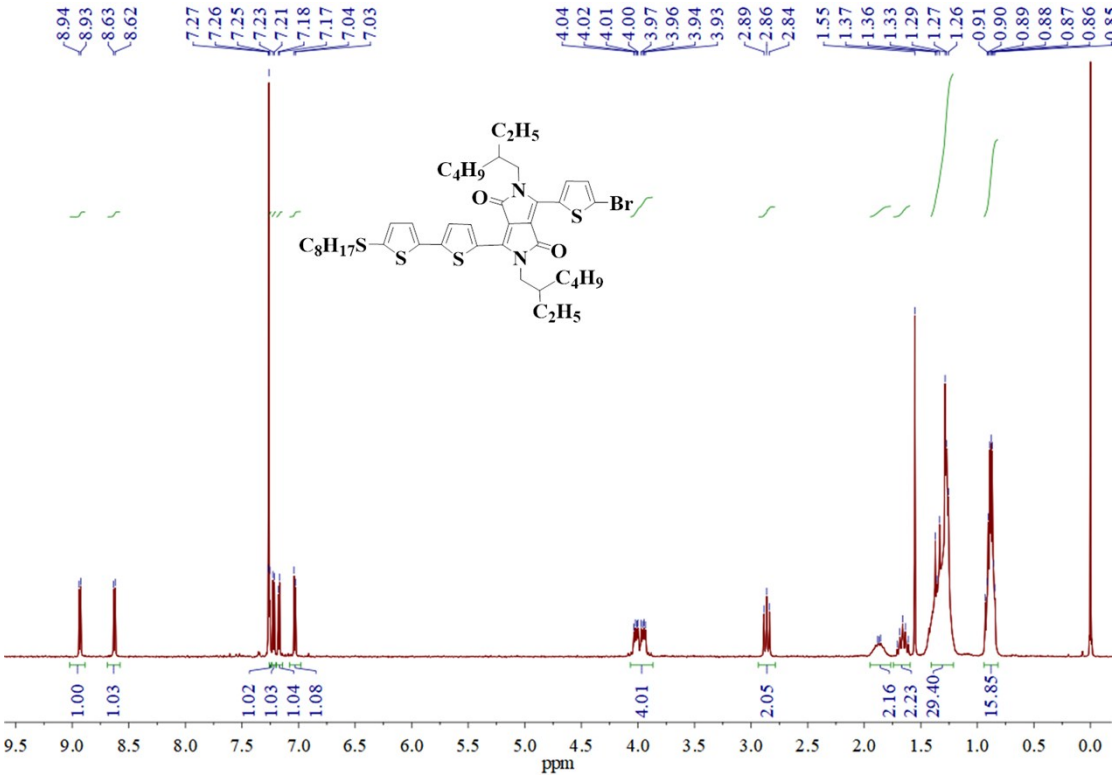

Fig.S7. [1]H NMR spectrum of DPP-TS.

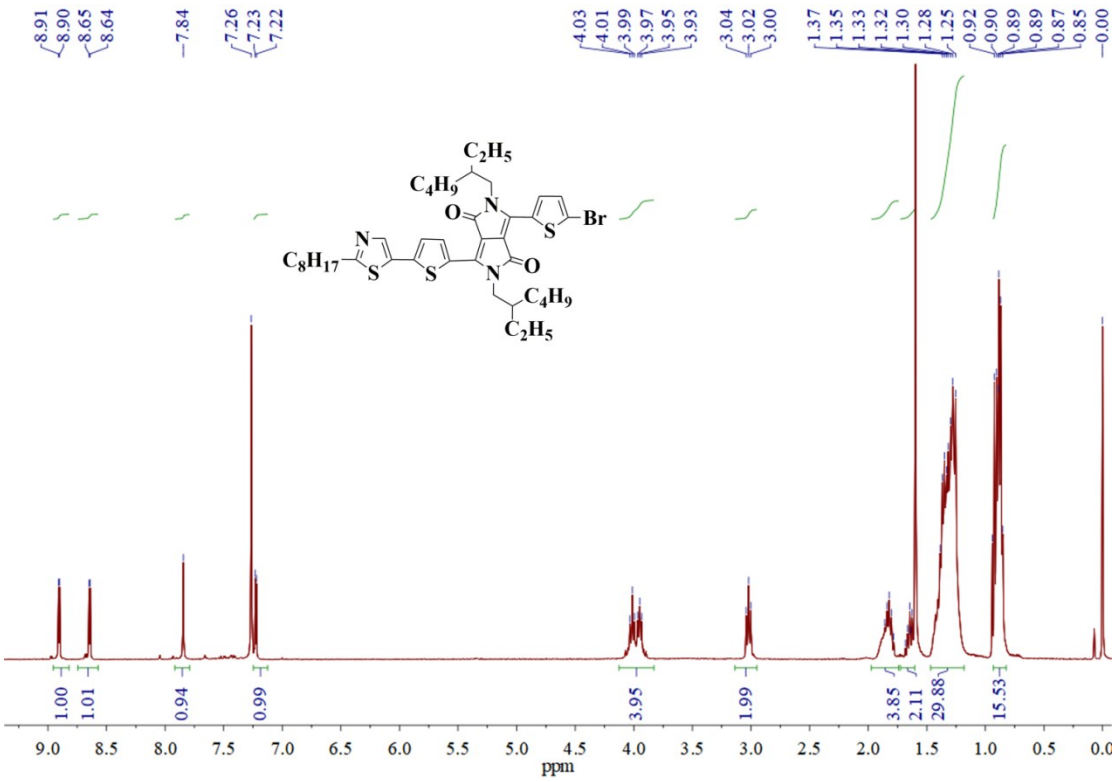

Fig.S8. [1]H NMR spectrum of DPP-TZ.

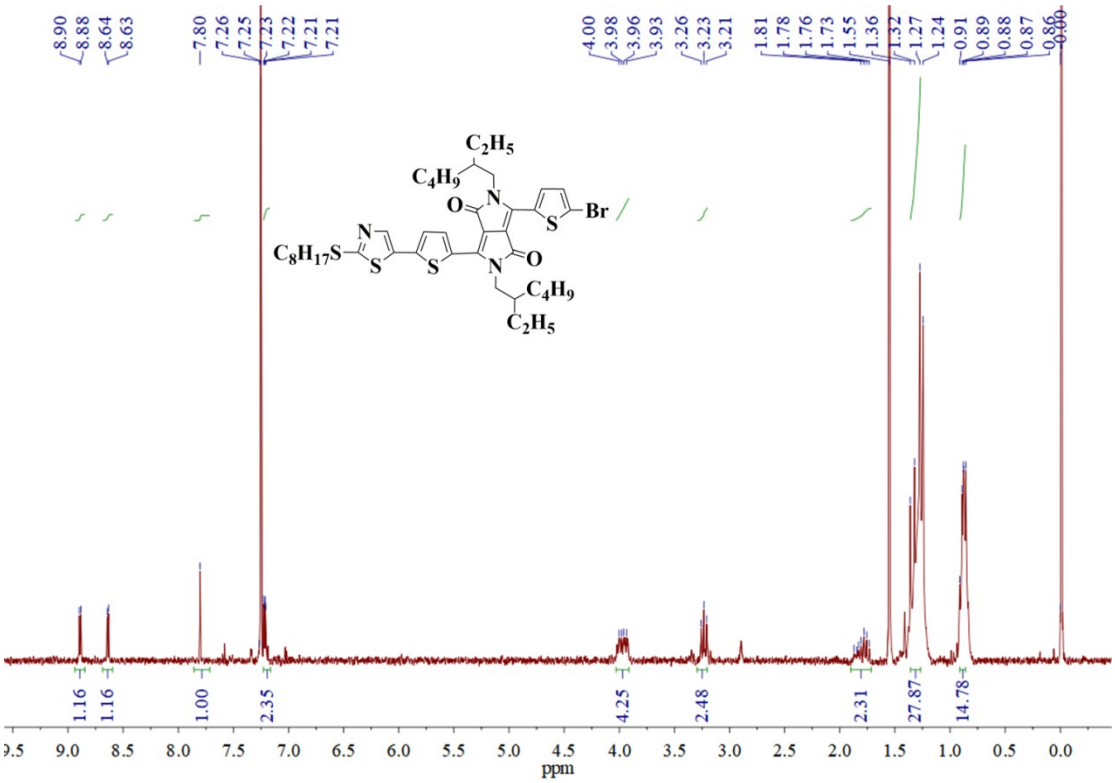

Fig.S9. [1]H NMR spectrum of DPP-TZS

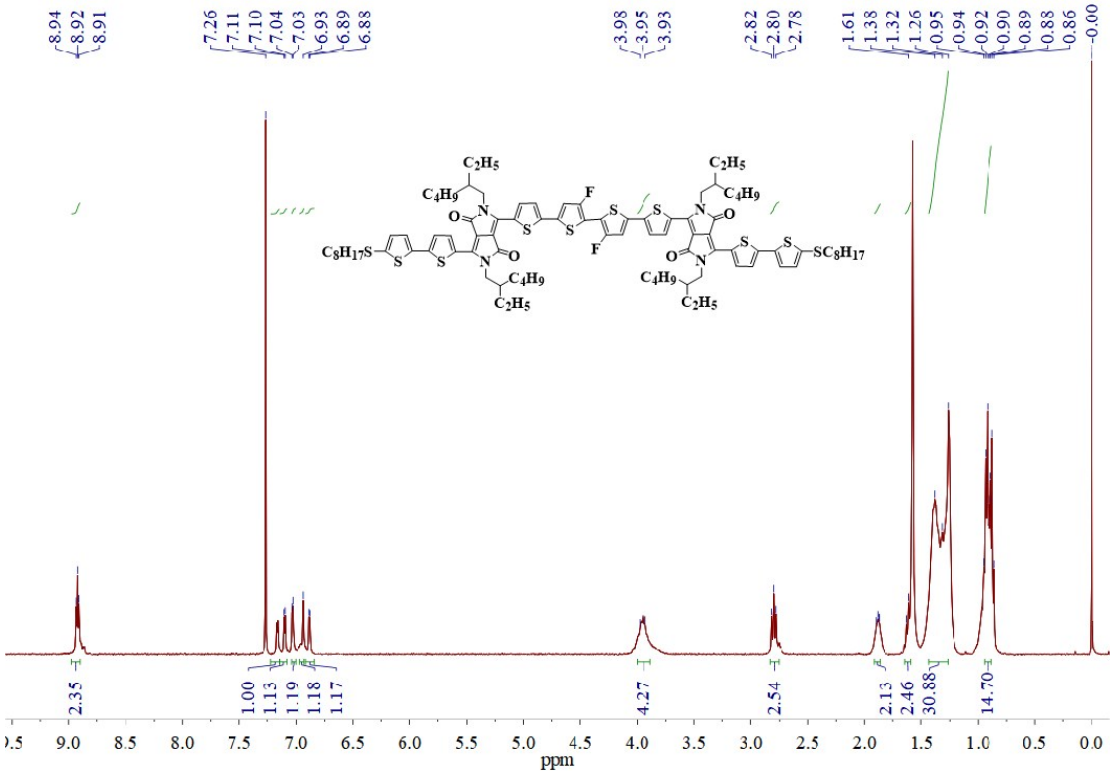

Fig.S10. [1]H NMR spectrum of DFT(TDPP-TS)$_2$.

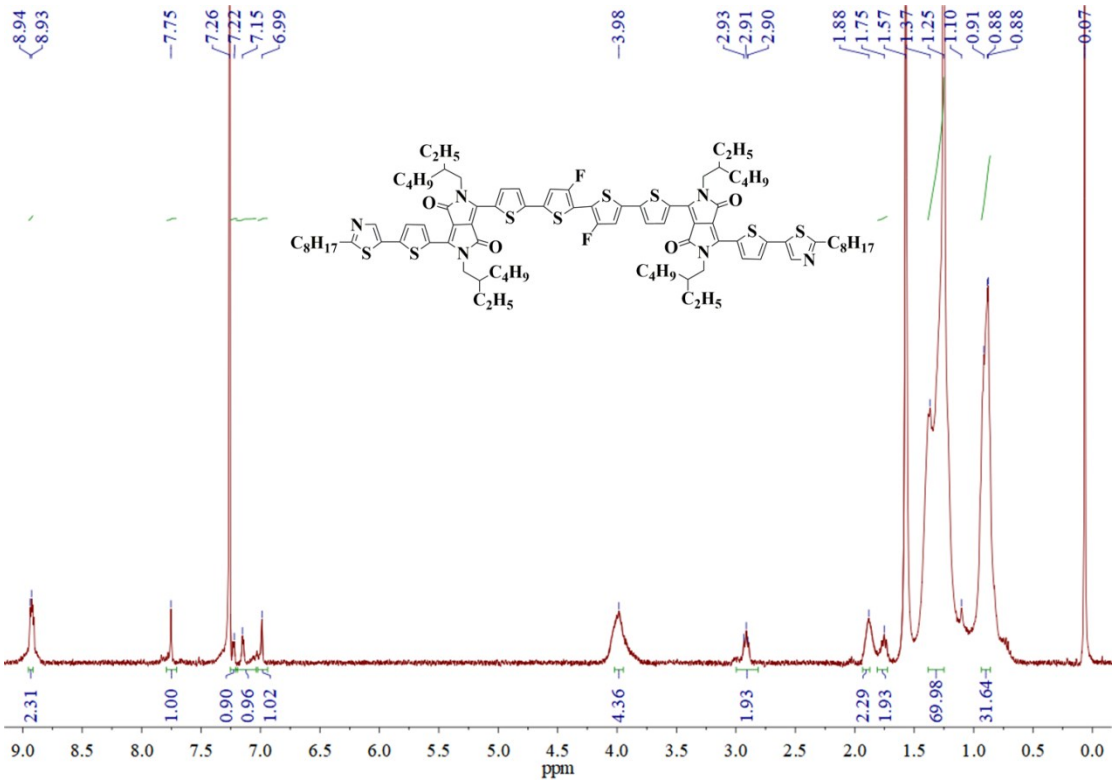

Fig.S11. ^{1}H NMR spectrum of DFT(TDPP-TZ)$_2$

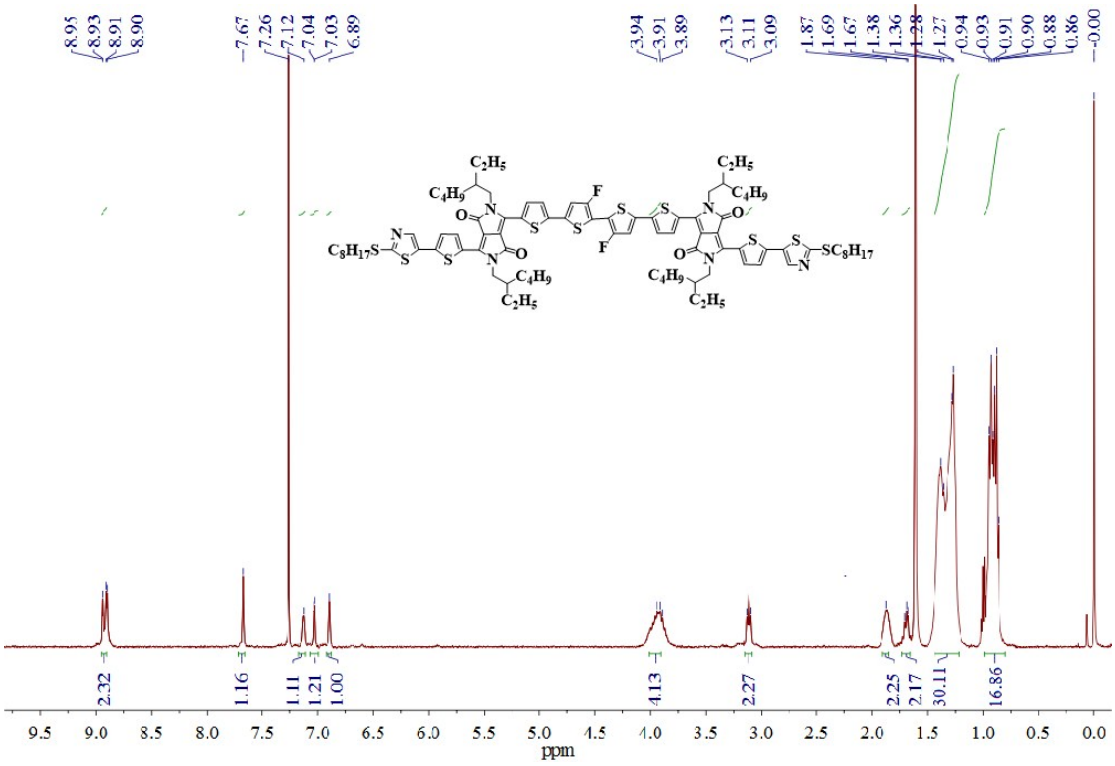

Fig. S12. ^{1}H-NMR spectrum of DFT(TDPP-TZS)$_2$

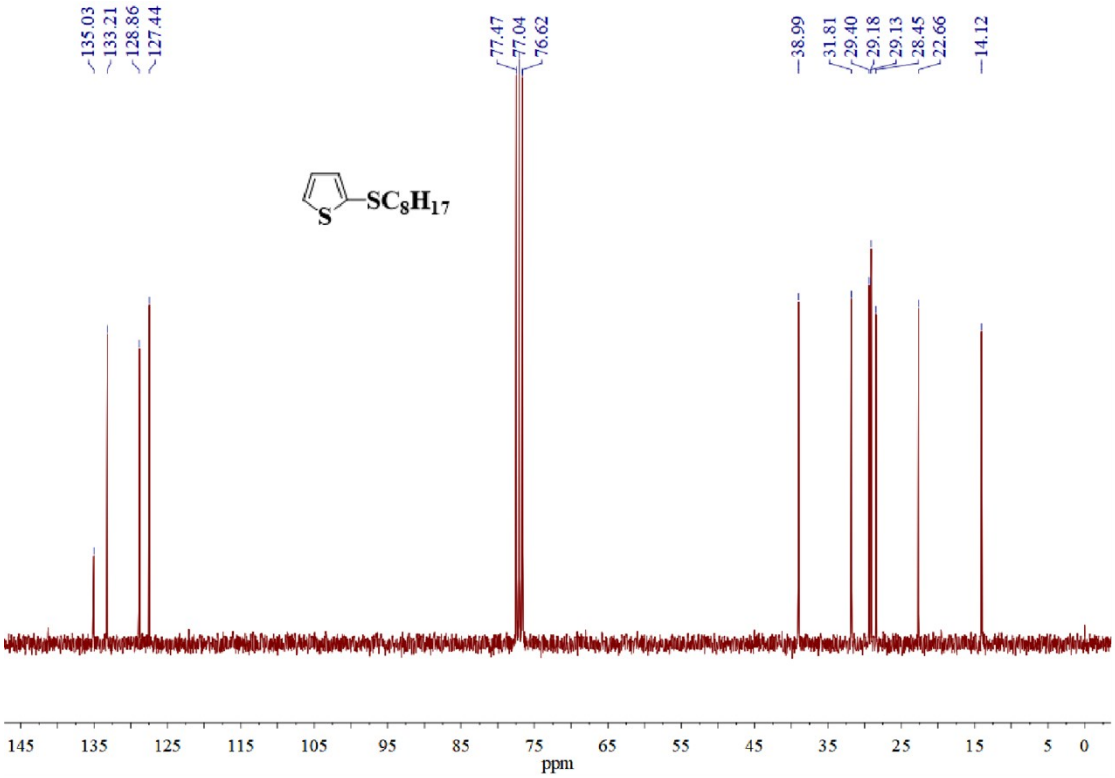

Fig. S13. ^{13}C-NMR spectrum of TS-R1.

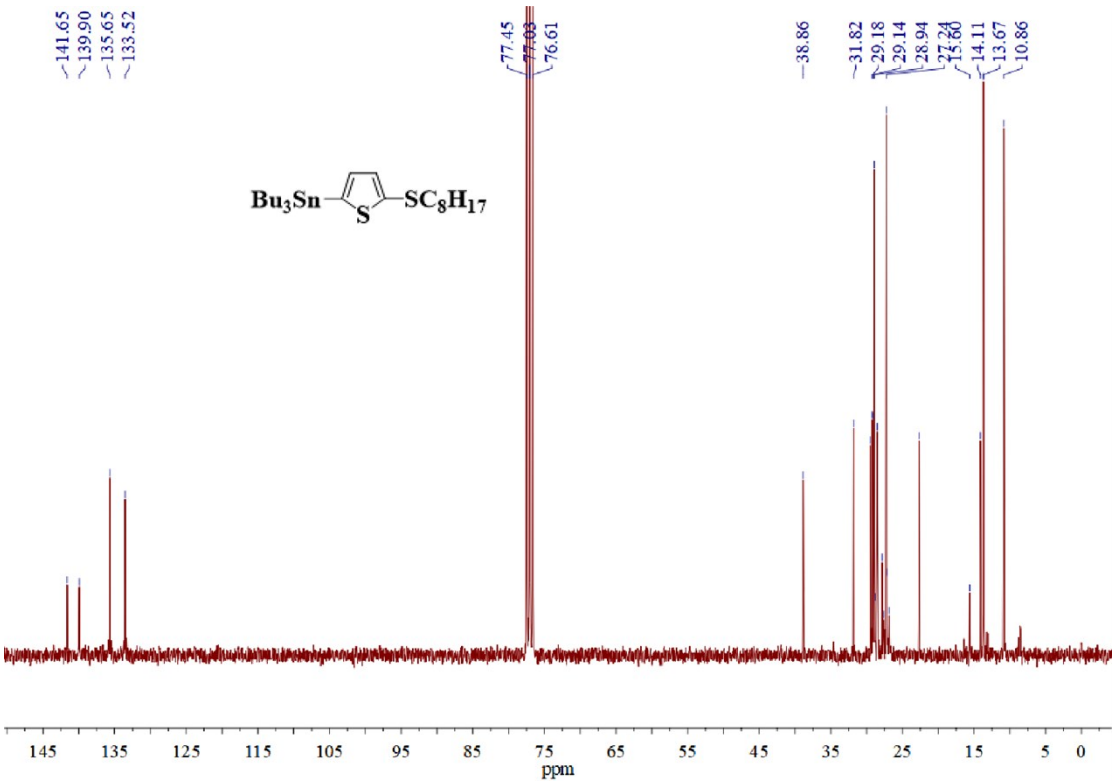

Fig. S14. ^{13}C-NMR spectrum of TS-Sn-R1.

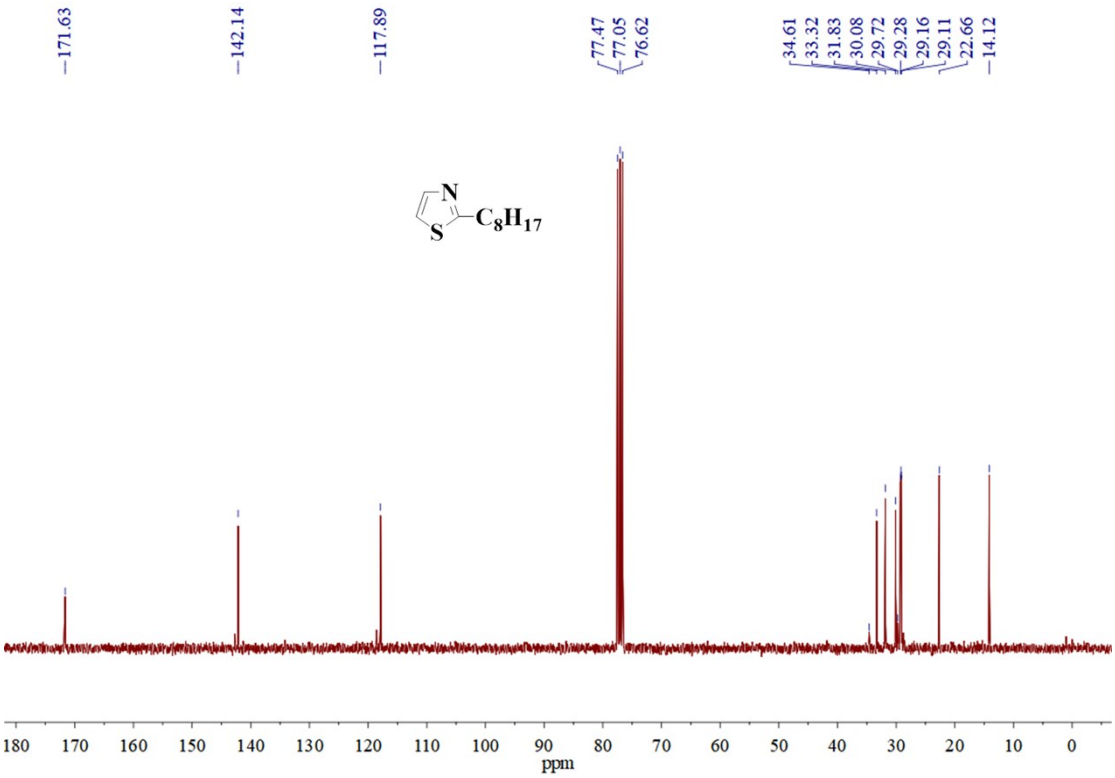

Fig. S15. ^{13}C-NMR spectrum of Tz-R1.

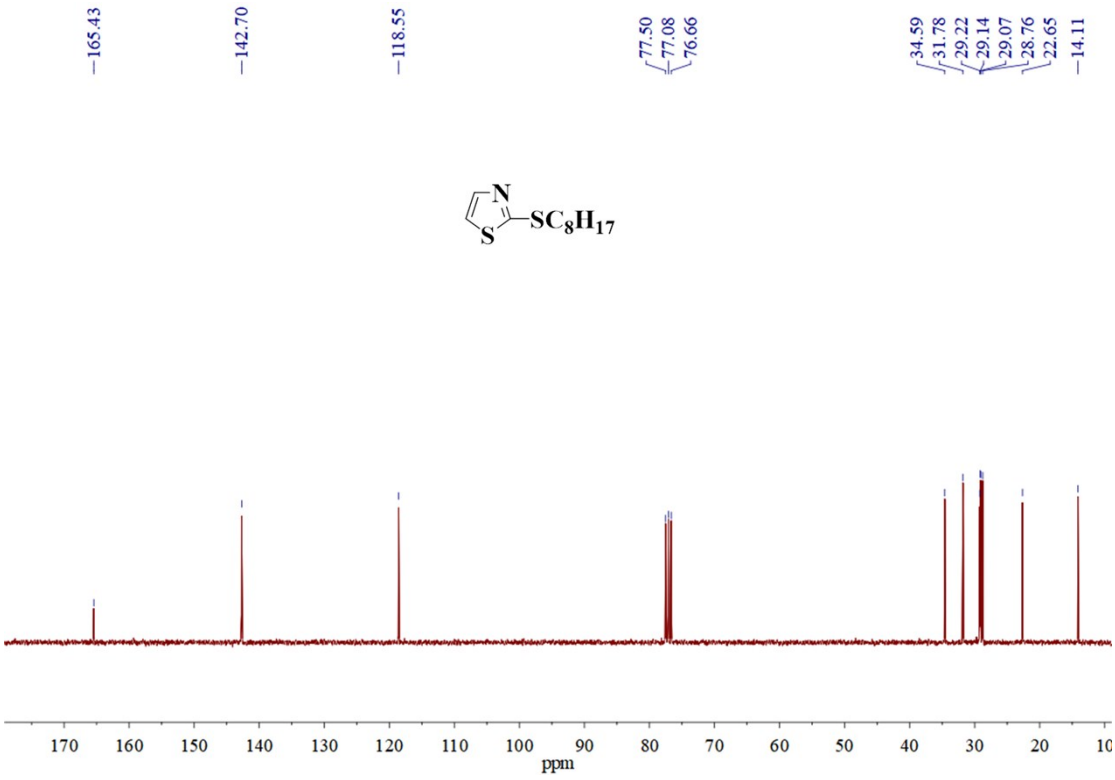

Fig. S16. ^{13}C-NMR spectrum of TZS-R1.

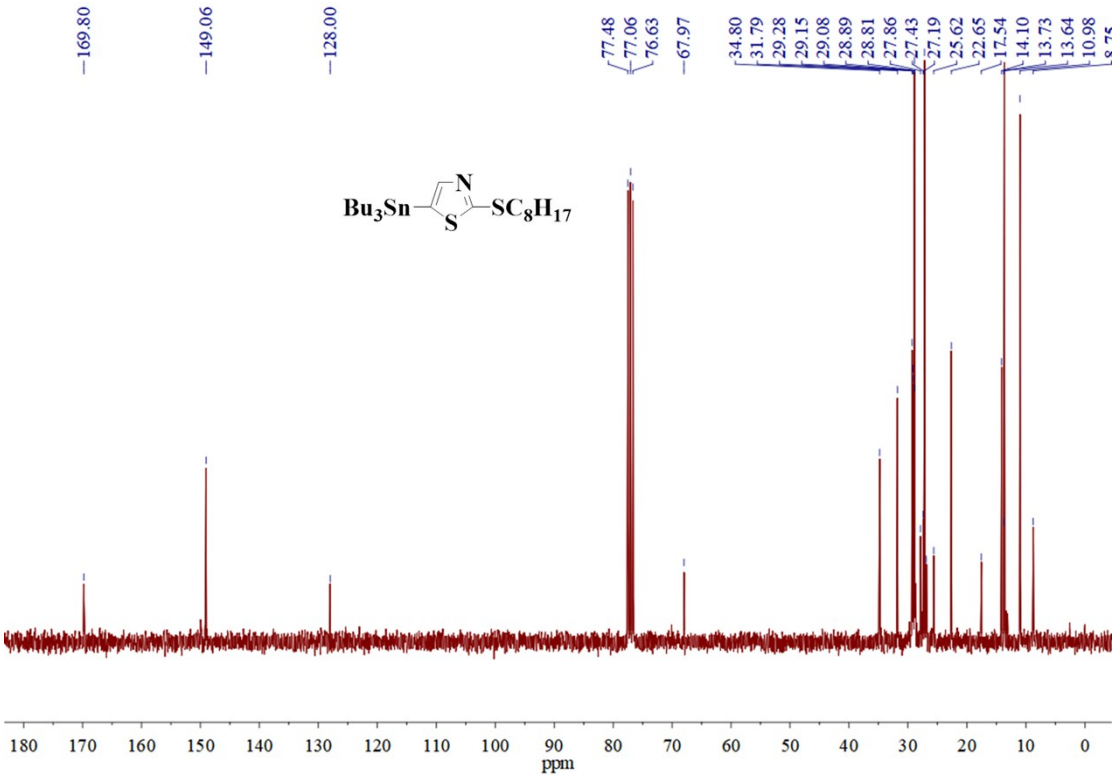

Fig. S17. ^{13}C-NMR spectrum of TZS-Sn-R1.

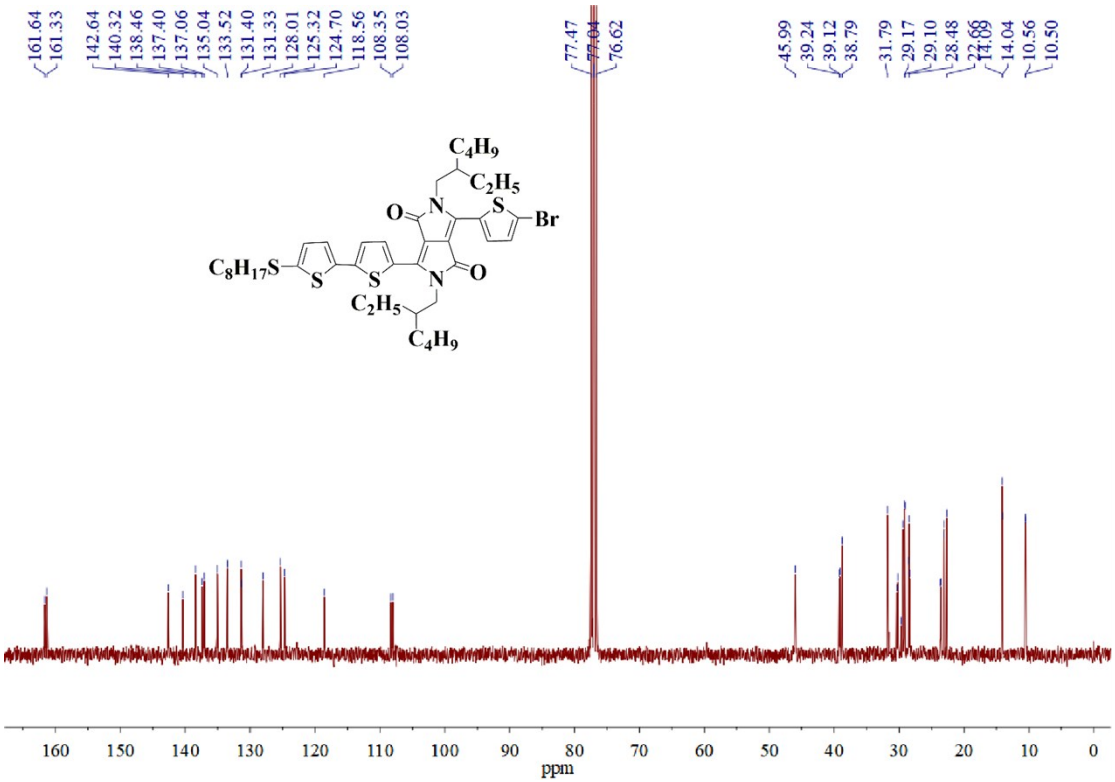

Fig.S18. ^{13}C-NMR spectrum of DPP-TS.

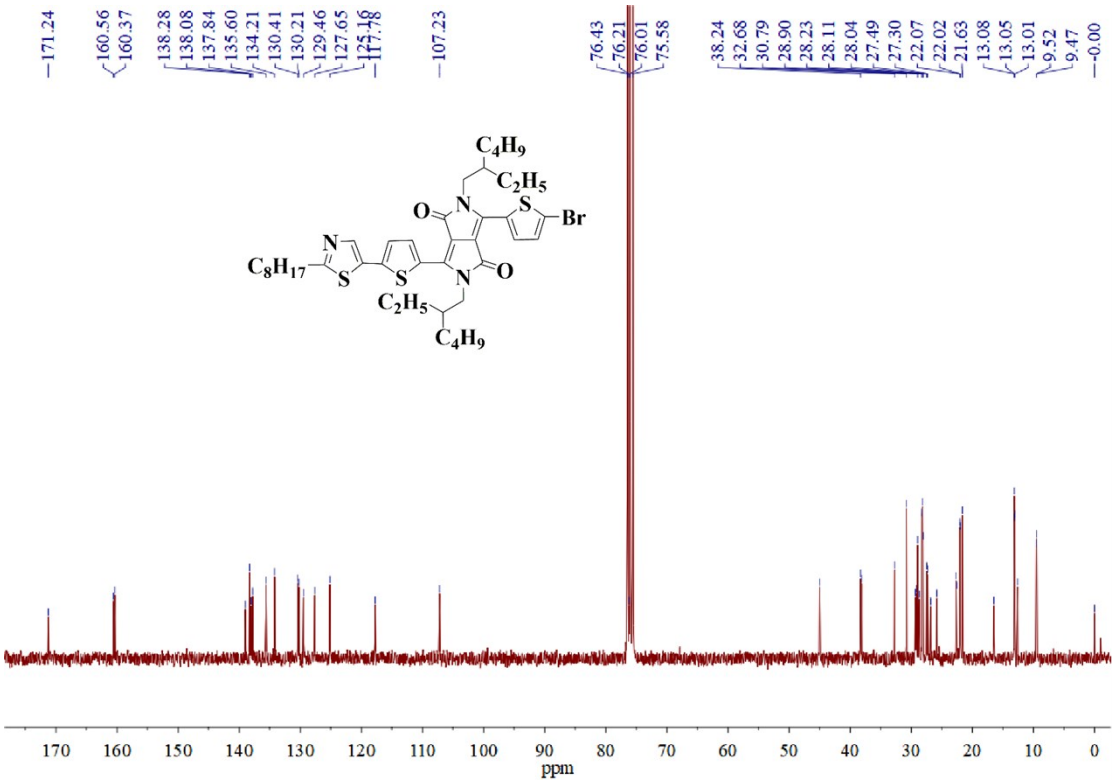

Fig.S19. ^{13}C-NMR spectrum of DPP-TZ.

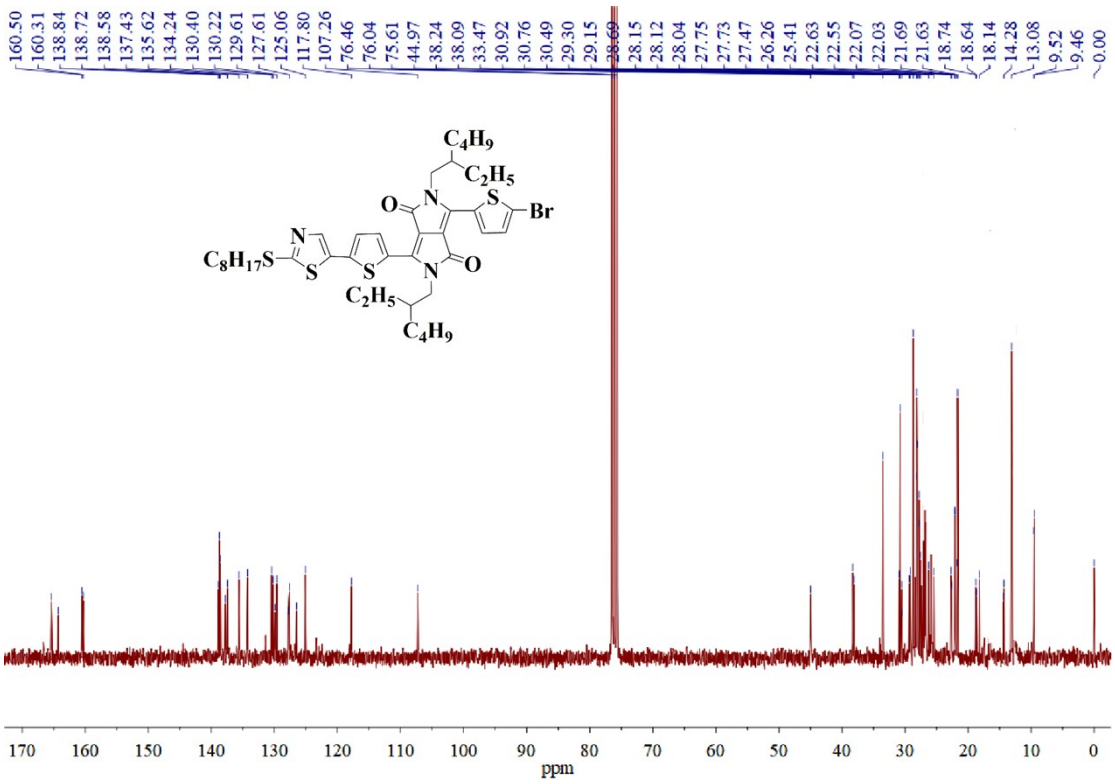

Fig.S20. ^{13}C-NMR spectrum of DPP-TZS.

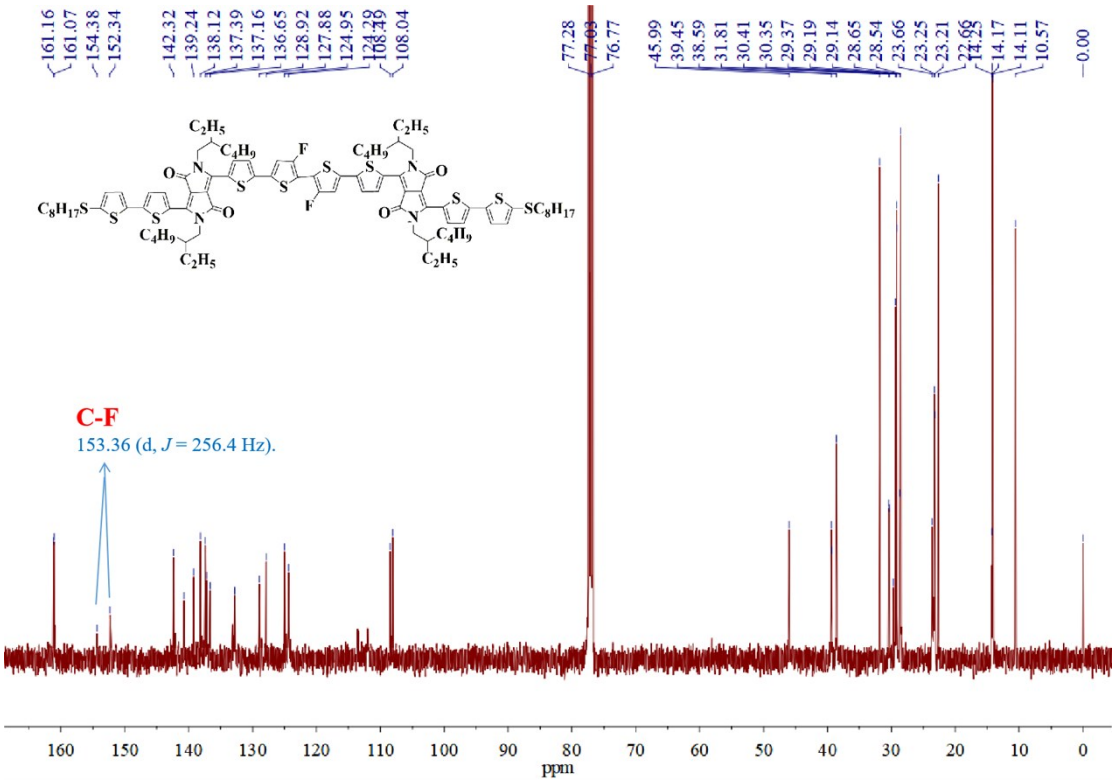

Fig. S21. ^{13}C-NMR spectrum of DFT(TDPP-TS)$_2$

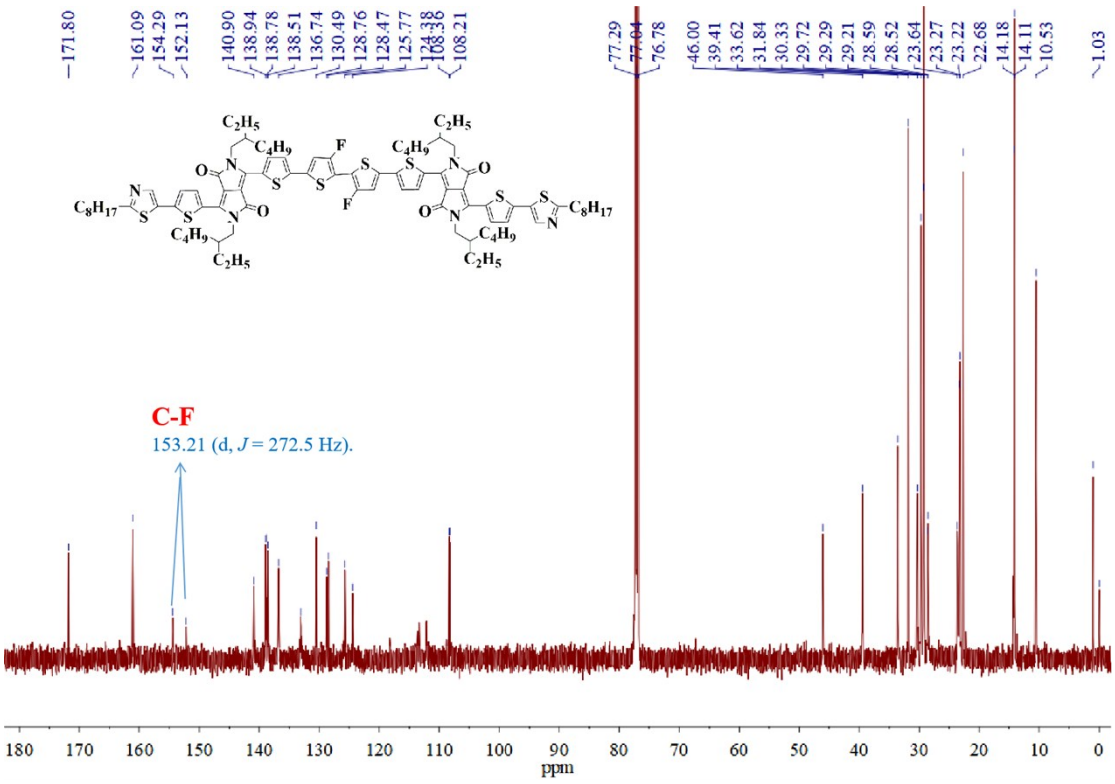

Fig. S22. ^{13}C-NMR spectrum of DFT(TDPP-TZ)$_2$

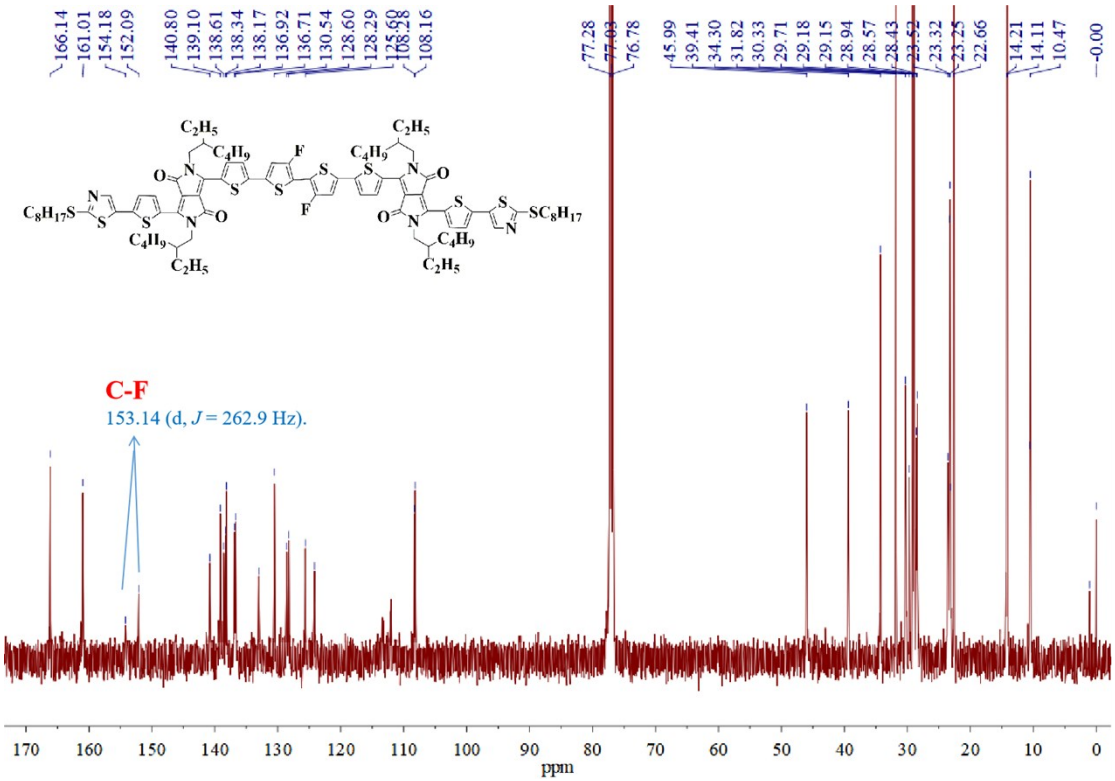

Fig. S23. ^{13}C-NMR spectrum of DFT(TDPP-TZS)$_2$

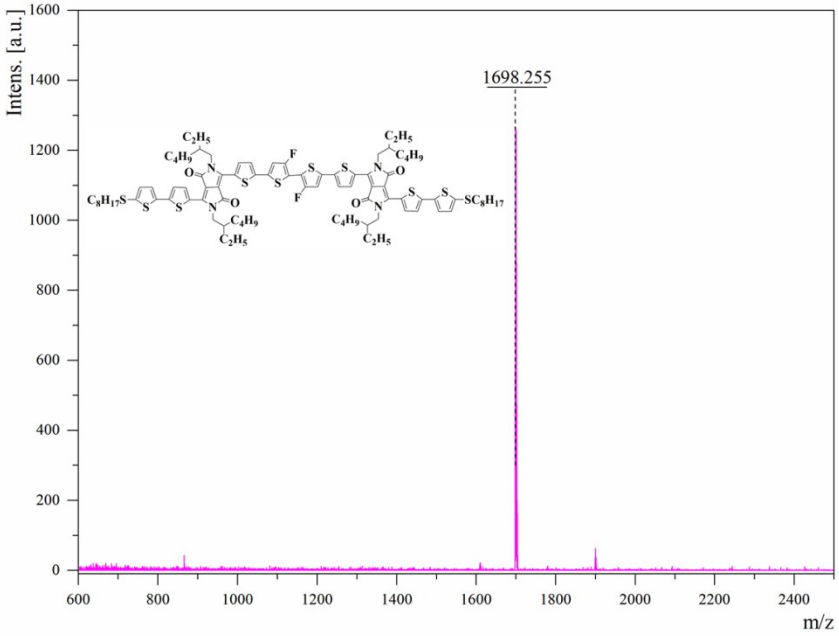

Fig. S24. MALDI-TOF MS Spectrum of DFT(TDPP-TS)$_2$

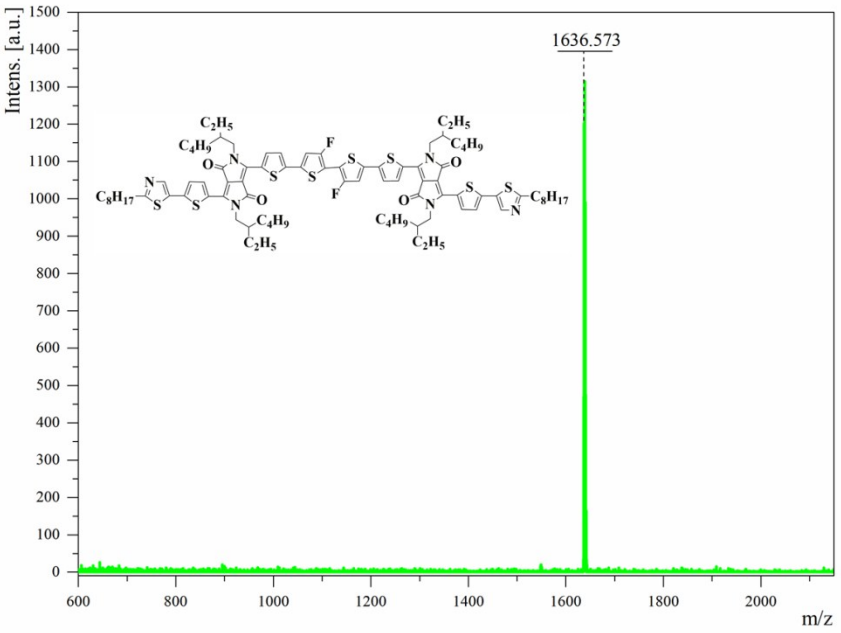

Fig. S25. MALDI-TOF MS Spectrum of DFT(TDPP-TZ)$_2$

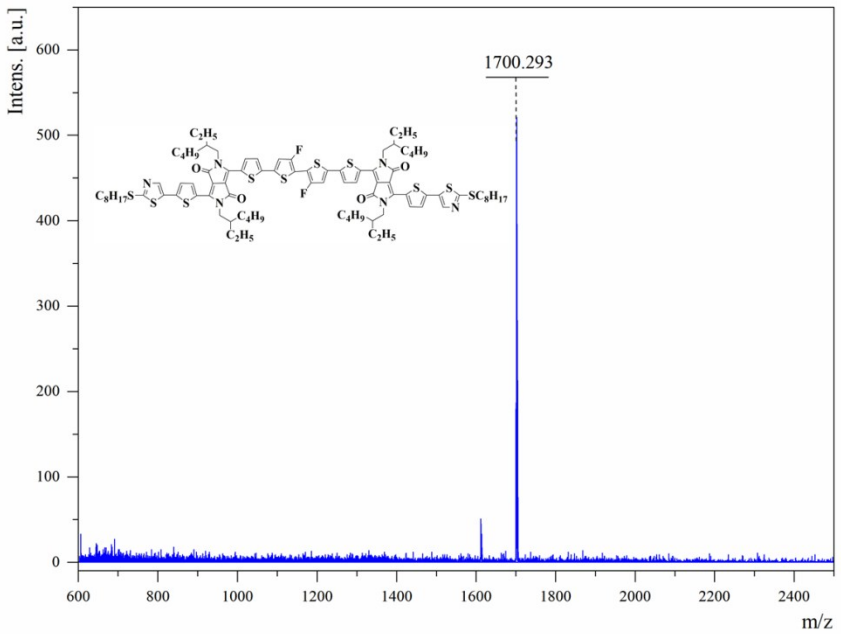

Fig. S26. MALDI-TOF MS Spectrum of DFT(TDPP-TZS)$_2$

3. The absorption molar coefficient in solution.

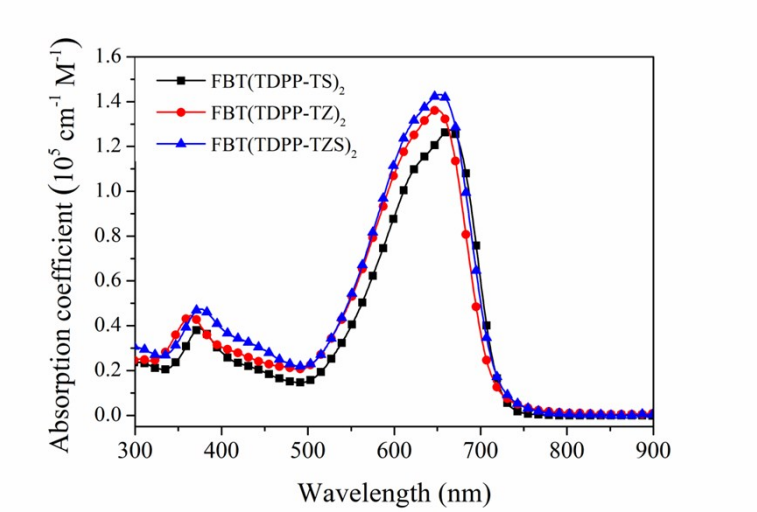

Fig.S27. Absorption spectra of SMs in dilute $CHCl_3$, respectively.

4. The Simulated absorption spectrum

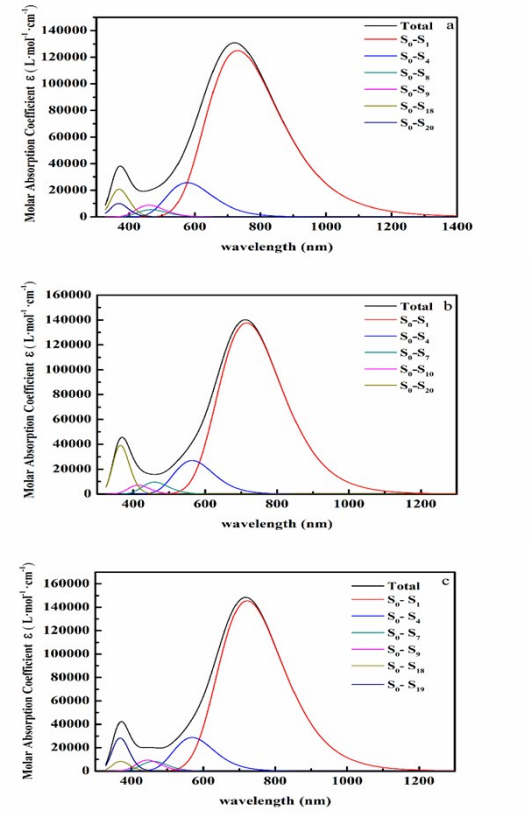

Fig.S28. Simulated absorption spectrum of a) FBT(TDPP-TS)$_2$, b) FBT(TDPP-TZ)$_2$, c) FBT(TDPP-TZS)$_2$, respectively.

5. Fabrication and characterization of organic solar cells

A sandwich structure of: ITO/PEDOT:PSS(5000 rpm, 140 °C 30min)/SMs:$PC_{71}BM$) (2000 rpm)/Ca (10 nm)/Al (100 nm), was used in the solar cells. The photosensitive layer was subsequently prepared by spin-coating rate of 2000 rpm with a solution of the SM/$PC_{71}BM$ (1:1, *w/w*) at room temperature in chloroform (CF) with 0.4% CN (CN/CF, v/v) on the PEDOT:PSS layer with a typical concentration of 12 mg mL^{-1}, followed by CS_2-SVA treatment for 30 s. Ca (10 nm) and Al (100 nm) were successively deposited on the photosensitive layer in vacuum and used as top electrodes. The current-voltage (*I–V*) characterization of the devices was carried out on a computer-controlled Keithley source measurement system. A solar simulator was used as the light source and the light intensity was monitored by a standard Si solar cell. The active area was 0.1 cm^2 for each cell. The thicknesses of the spun-cast films were recorded by a profilometer (Alpha-Step 200, Tencor Instruments). The external quantum efficiency (*EQE*) was measured with a Stanford Research Systems model SR830 DSP lock-in amplifier coupled with WDG3 monochromator and a 150 W xenon lamp.

6. Photovoltaic properties of the FBT(TDPP-TS)$_2$/$PC_{71}BM$-based OPV cells.

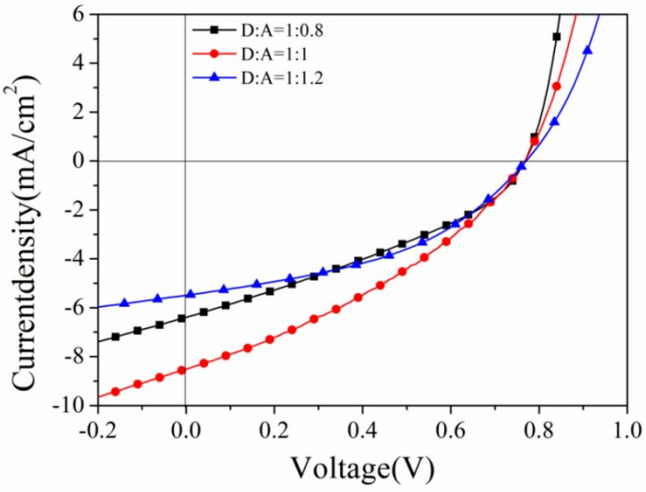

Fig. S29. *J-V* curve of the FBT(TDPP-TS)$_2$/$PC_{71}BM$-based OSCs under AM.1.5G illumination (100 mW/cm^2) with SM/$PC_{71}BM$ D:A ratios optimization.

Table S1. Photovoltaic parameters of the FBT(TDPP-TS)$_2$/PC$_{71}$BM-based PSCs under AM.1.5G illumination (100 mW/cm^2) with SM/PC$_{71}$BM D:A ratios optimization.

D:A	V_{oc}(V)	J_{sc}(mA/cm^2)	FF(%)	PCE(%)
1:0.8	0.76	6.39	34.18	1.66
1:1	0.76	8.51	34.63	2.24
1:1.2	0.76	5.47	43.29	1.80

Device condition: (1) chloroform(CF); (2) concentration: 12 mg/mL of FBT(TDPP-TS)$_2$ in CF; (3) Structure: ITO/PEDOT:PSS(5000 rpm, 140 °C 30min)/SMs:PC$_{71}$BM) (2000 rpm)/Ca (10 nm)/Al (100 nm); (4) Spin-coating temperature：at room temperature.

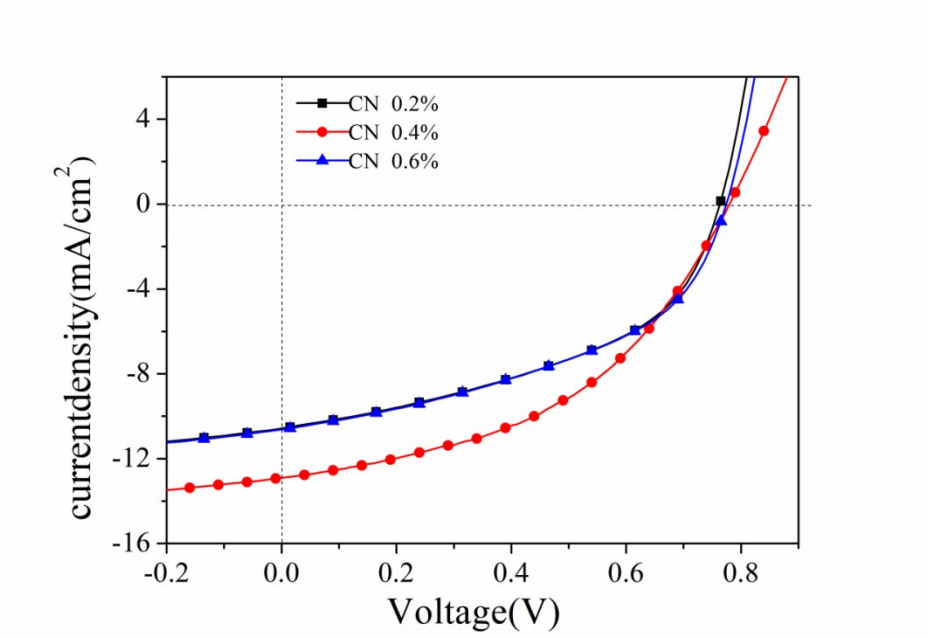

Fig. S30. *J-V* curve of the FBT(TDPP-TS)$_2$/PC$_{71}$BM-based OSCs under AM.1.5G illumination (100 mW/cm^2) with SM/PC$_{71}$BM CN ratios optimization.

Table S2. Photovoltaic parameters of the FBT(TDPP-TS)$_2$/PC$_{71}$BM-based PSCs under AM.1.5G illumination (100 mW/cm^2) with SM/PC$_{71}$BM CN ratios optimization.

CN	V_{oc}(V)	J_{sc}(mA/cm^2)	FF(%)	PCE(%)
0.2%	0.765	10.63	46.13	3.75
0.4%	0.77	12.9	46.06	4.58
0.6%	0.75	10.6	47.06	3.73

Device condition: (1) chloroform(CF); (2) concentration: 12 mg/mL of FBT(TDPP-TS)$_2$ in CF; (3) Structure:ITO/PEDOT:PSS(5000 rpm, 140 ^{o}C 30min)/SMs:PC$_{71}$BM) (2000 rpm)/Ca (10 nm)/Al (100 nm). (4) Spin-coating temperature：at room temperature.

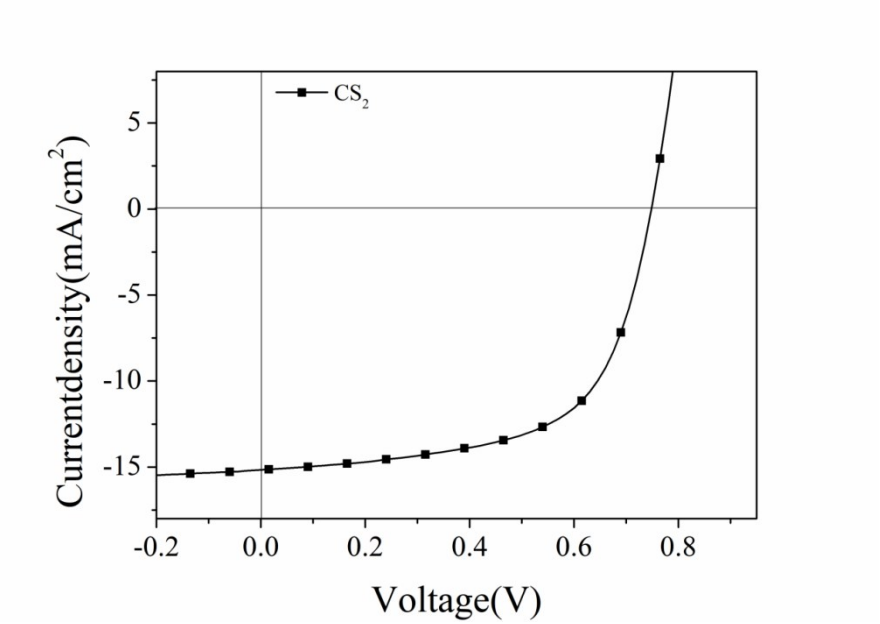

Fig. S31. *J-V* curve of the FBT(TDPP-TS)$_2$/PC$_{71}$BM-based SM-OSCs under AM.1.5G illumination (100 mW/cm^2) with CS_2 solvent anealing.

Table. S3. *J-V* curve of the FBT(TDPP-TS)$_2$/PC$_{71}$BM-based SM-OSCs under

AM.1.5G illumination (100 mW/cm^2) with CS_2 solvent anealing.

Solvent	V_{oc}(V)	J_{sc}(mA/cm^2)	FF(%)	PCE(%)
CS_2	0.735	15.16	62.47	6.96

Device condition: (1) chloroform (CF); (2) concentration:ITO/PEDOT:PSS(5000 rpm, 140 °C 30min)/SMs:$PC_{71}BM$) (2000 rpm)/Ca (10 nm)/Al (100 nm); (3) Solvent vapor annealing time: 30 s

7. Photovoltaic properties of the FBT(TDPP-TZ)$_2$/$PC_{71}BM$-based OPV cells.

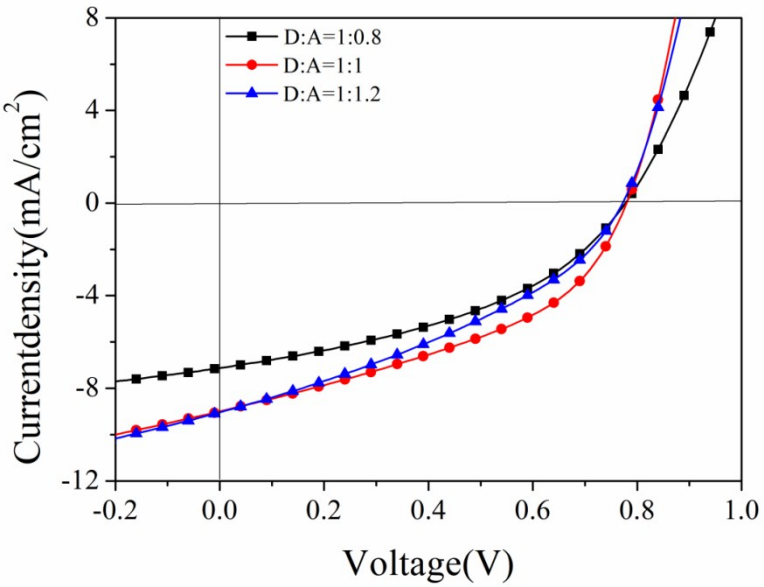

Fig. S32. *J-V* curve of the FBT(TDPP-TZ)$_2$/$PC_{71}BM$-based SM-OSCs under AM.1.5G illumination (100 mW/cm^2) with D:A ratios optimization.

Table. S4. *J-V* curve of the FBT(TDPP-TZ)$_2$/$PC_{71}BM$-based SM-OSCs under

AM.1.5G illumination (100 mW/cm^2) with D:A ratios optimization.

D:A	V_{oc}(V)	J_{sc}(mA/cm^2)	FF(%)	PCE(%)
1:0.8	0.77	7.12	41.77	2.29
1:1	0.77	8.99	42.47	2.94
1:1.2	0.77	9.04	36.06	2.51

Device condition: (1) chloroform(CF); (2) concentration: 12 mg/mL of FBT(TDPP-TZ)$_2$ in CF; (3) Structure: ITO/PEDOT:PSS(5000 rpm, 140 ^{o}C 30min)/ SMs: $PC_{71}BM$) (2000 rpm)/Ca (10 nm)/Al (100 nm); (4) Spin-coating temperature：at room temperature.

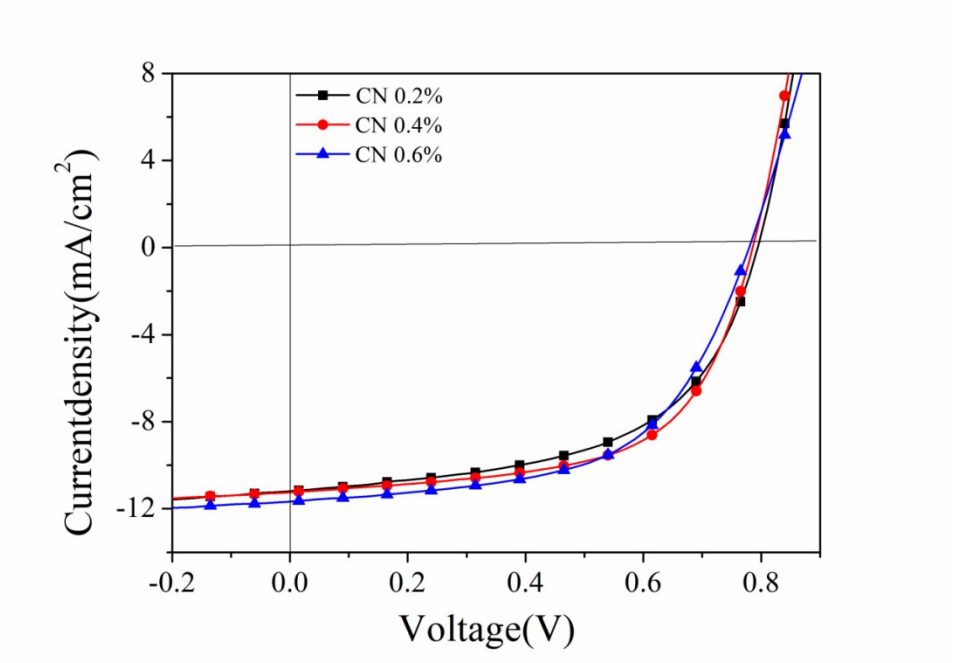

Fig. S33. *J-V* curve of the FBT(TDPP-TZ)$_2$/$PC_{71}BM$-based SM-OSCs under AM.1.5G illumination (100 mW/cm^2) with CN ratios optimization.

Table. S5. *J-V* curve of the FBT(TDPP-TZ)$_2$/$PC_{71}BM$-based SM-OSCs under

AM.1.5G illumination (100 mW/cm^2) with CN ratios optimization.

CN	V_{oc}(V)	J_{sc}(mA/cm^2)	FF(%)	PCE(%)
0.2%	0.78	11.20	56.15	4.90
0.4%	0.78	11.24	60.58	5.31
0.6%	0.77	11.67	57.95	5.17

Device condition: (1) chloroform(CF); (2) concentration: 12 mg/mL of FBT(TDPP-TZ)$_2$ in CF; (3) Structure: ITO/PEDOT:PSS(5000 rpm, 140 ^{o}C 30min)/ SMs: $PC_{71}BM$) (2000 rpm)/Ca (10 nm)/Al (100 nm); (4) Spin-coating temperature：at room temperature.

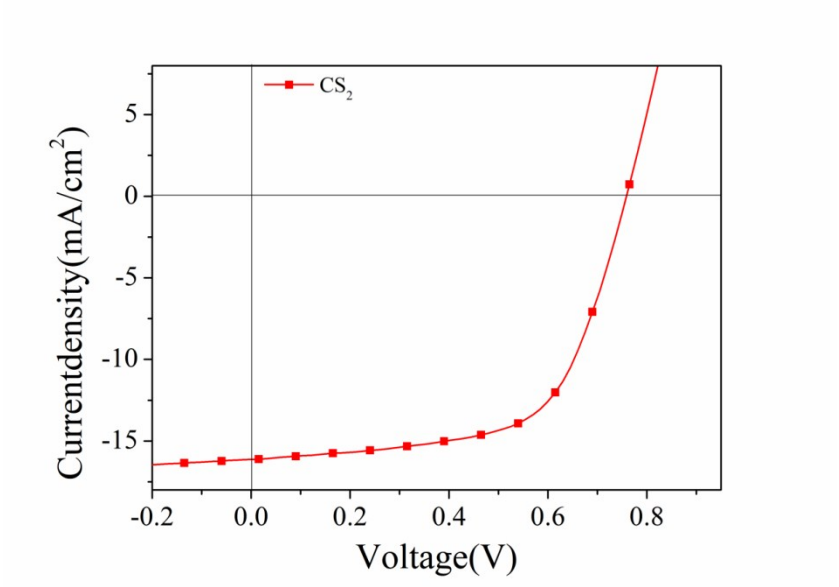

Fig. S34. *J-V* curve of the FBT(TDPP-TZ)$_2$/$PC_{71}BM$-based SM-OSCs under AM.1.5G illumination (100 mW/cm^2) with CS_2 solvent annealing.

Table. S6. *J-V* curve of the FBT(TDPP-TZ)$_2$/$PC_{71}BM$-based SM-OSCs under

AM.1.5G illumination (100 mW/cm^2) with CS_2 solvent annealing.

Solvent	V_{oc}(V)	J_{sc}(mA/cm^2)	FF(%)	PCE(%)
THF	0.75	16.12	63.09	7.63

Device condition: (1) chloroform (CF); (2) concentration: ITO/PEDOT:PSS(5000 rpm, 140 °C 30min)/ SMs: $PC_{71}BM$) (2000 rpm)/Ca (10 nm)/Al (100 nm); (3) Solvent vapor annealing time: 30 s

5. Photovoltaic properties of the FBT(TDPP-TZS)$_2$/PC$_{71}$BM-based OPV cells.

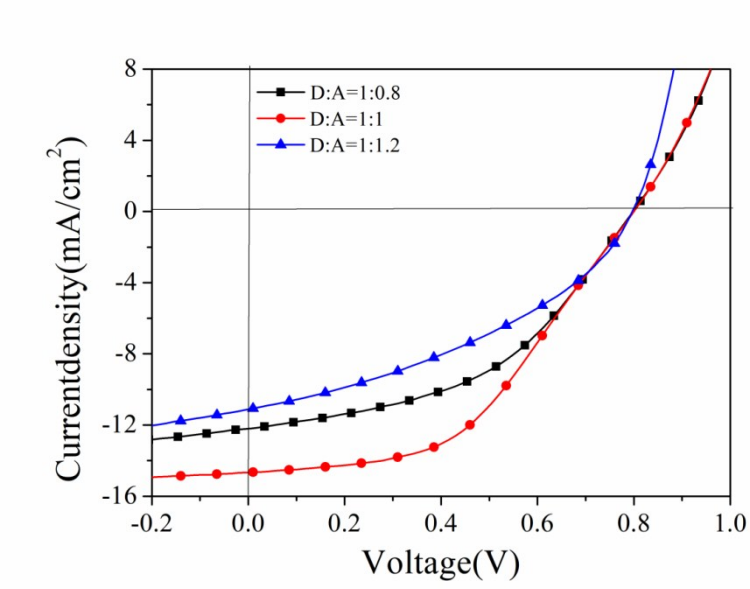

Fig. S35. *J-V* curve of the FBT(TDPP-TZS)$_2$/$PC_{71}BM$-based OSCs under AM.1.5G illumination (100 mW/cm^2) with SM/$PC_{71}BM$ D:A ratios optimization.

Table. S7. *J-V* curve of the FBT(TDPP-TZS)$_2$/$PC_{71}BM$-based SM-OSCs under

AM.1.5G illumination (100 mW/cm^2) with D:A ratios optimization.

D:A	V_{oc}(V)	J_{sc}(mA/cm^2)	FF(%)	PCE(%)
1:0.8	0.79	12.18	46.56	4.48
1:1	0.79	14.65	47.70	5.52
1:1.2	0.79	11.07	39.22	3.43

Device condition: (1) chloroform(CF); (2) concentration: 12 mg/mL of FBT(TDPP-TZS)$_2$ in CF; (3) Structure: ITO/PEDOT:PSS(5000 rpm, 140 ^{o}C 30min)/ SMs: PC$_{71}$BM) (2000 rpm)/Ca (10 nm)/Al (100 nm); (4) Spin-coating temperature：at room temperature.

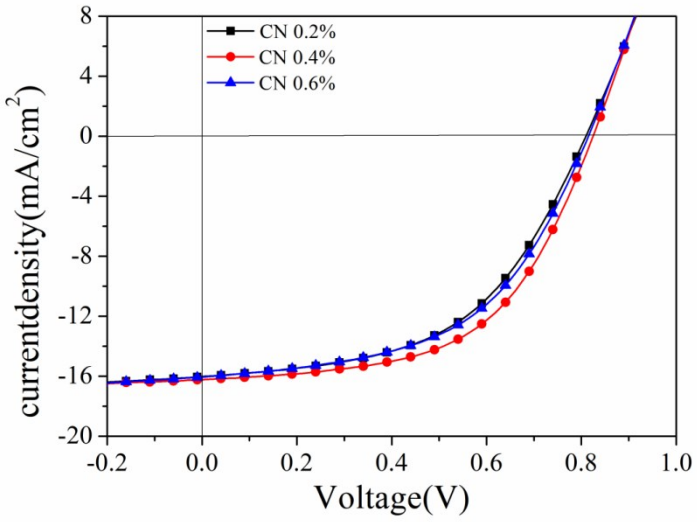

Fig. S36. *J-V* curve of the FBT(TDPP-TZS)$_2$/PC$_{71}$BM-based OSCs under AM.1.5G illumination (100 mW/cm^2) with SM/PC$_{71}$BM CN ratios optimization.

Table. S8. *J-V* curve of the FBT(TDPP-TZS)$_2$/PC$_{71}$BM-based SM-OSCs under

AM.1.5G illumination (100 mW/cm^2) with CN ratios optimization.

CN	V_{oc}(V)	J_{sc}(mA/cm^2)	FF(%)	PCE(%)
0.2%	0.80	16.02	52.23	6.69
0.4%	0.82	16.23	55.58	7.40
0.6%	0.81	16.06	52.47	6.82

Device condition: (1) chloroform(CF); (2) concentration: 12 mg/mL of FBT(TDPP-TZS)$_2$ in CF; (3) Structure: ITO/PEDOT:PSS(5000 rpm, 140 ^{o}C 30min)/ SMs: $PC_{71}BM$) (2000 rpm)/Ca (10 nm)/Al (100 nm); (4) Spin-coating temperature：at room temperature.

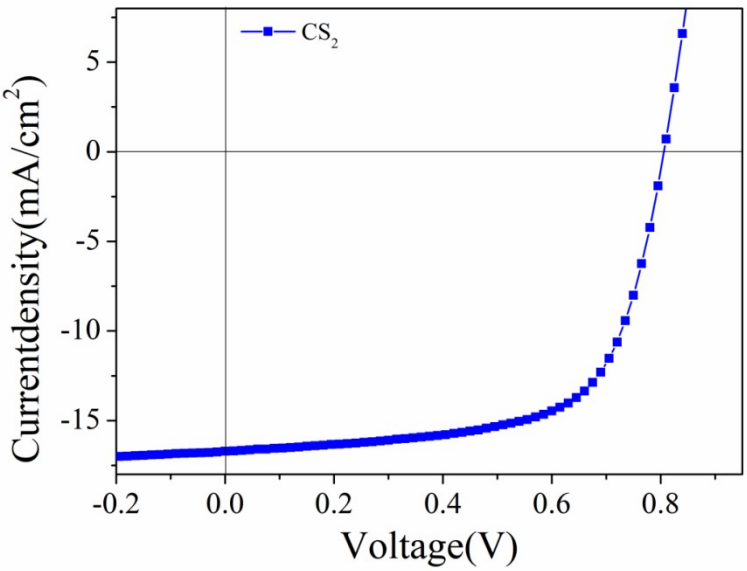

Fig. S37. *J-V* curve of the FBT(TDPP-TZS)$_2$/$PC_{71}BM$-based SM-OSCs under AM.1.5G illumination (100 mW/cm^2) with CS_2 solvent annealing.

Table. S9. *J-V* curve of the FBT(TDPP-TZS)$_2$/$PC_{71}BM$-based SM-OSCs under

AM.1.5G illumination (100 mW/cm^2) with CS_2 solvent annealing.

Solvent	**V_{oc}(V)**	**J_{sc}(mA/cm^2)**	**FF(%)**	**PCE(%)**
CS_2	0.80	16.75	66.93	8.91

Device condition: (1) chloroform (CF); (2) concentration: ITO/PEDOT:PSS(5000 rpm, 140 ^oC 30min)/ SMs: $PC_{71}BM$) (2000 rpm)/Ca (10 nm)/Al (100 nm); (3) Solvent vapor annealing time: 30 s